

Factorized Video Generation: Decoupling Scene Construction and Temporal Synthesis in Text-to-Video Diffusion Models

Mariam Hassan*, Bastien Van Delft*, Wuyang Li, Alexandre Alahi
 École Polytechnique Fédérale de Lausanne (EPFL)
 firstname.lastname@epfl.ch

Abstract

State-of-the-art Text-to-Video (T2V) diffusion models can generate visually impressive results, yet they still frequently fail to compose complex scenes or follow logical temporal instructions. In this paper, we argue that many errors, including apparent motion failures, originate from the model’s inability to construct a semantically correct or logically consistent initial frame. We introduce Factorized Video Generation (FVG), a pipeline that decouples these tasks by decomposing the Text-to-Video generation into three specialized stages: (1) Reasoning, where a Large Language Model (LLM) rewrites the video prompt to describe only the initial scene, resolving temporal ambiguities; (2) Composition, where a Text-to-Image (T2I) model synthesizes a high-quality, compositionally-correct anchor frame from this new prompt; and (3) Temporal Synthesis, where a video model, finetuned to understand this anchor, focuses its entire capacity on animating the scene and following the prompt. Our decomposed approach sets a new state-of-the-art on the T2V CompBench benchmark and significantly improves all tested models on VBV2. Furthermore, we show that visual anchoring allows us to cut the number of sampling steps by 70% without any loss in performance, leading to a substantial speed-up in sampling. Factorized Video Generation offers a simple yet practical path toward more efficient, robust, and controllable video synthesis. Project website: <https://vita-epfl.github.io/FVG/>.

1. Introduction

Recent advances in text-to-video (T2V) diffusion models have substantially improved visual fidelity, temporal consistency, and prompt adherence [1, 3, 5, 11, 21, 26, 41, 49]. However, despite these achievements, current systems exhibit notable brittleness: they often generate visually convincing videos that nevertheless violate basic semantic con-

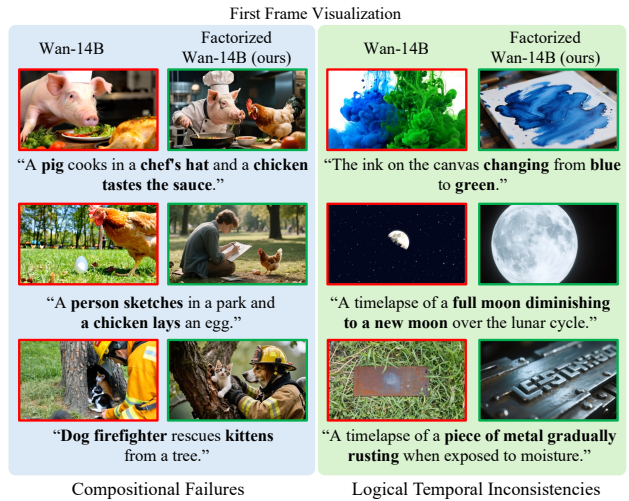


Figure 1. **Example failure modes in SoTA video generative foundational models.** We compare the first frame of videos from T2V Wan 2.2 [41] and our **Factorized** Wan 2.2. T2V Wan 2.2 composes scenes incorrectly and exhibits logical temporal inconsistencies, struggling to establish coherent scene structure without explicit visual grounding. This can be solved via our factorization.

straints in the prompt, particularly when the prompt requires binding specific actions to specific entities or maintaining a coherent logical sequence of events. These failures highlight persistent limitations in how existing models **jointly reason about language, scene structure, and temporal evolution** in a unified video generator.

Prior works have documented these compositional failures [15, 35, 39, 47, 51], showing that T2V models frequently misinterpret or only partially follow user instructions, especially when the prompts deviate from the curated, syntactically clean data used during training. A common mitigation is the **prompt extension**, which expands short or underspecified prompts using Large Language Models (LLMs) [8, 16, 18]. While such rewriting can increase textual specificity, it does not address the underlying representational issue: the model may still construct an incorrect

* Equal Contribution

scene or misrepresent the entities and relations described, regardless of how detailed the rewritten prompt becomes.

Our analysis across multiple state-of-the-art systems reveals that many errors originate in the model’s representation of the scene itself. In Figure 1, we observe that existing models routinely **(1) miscompose visual elements of the scene, and (2) generate initial states incompatible with the requested temporal evolution**. Once the scene composition violates the prompt semantics, the temporal modeling fails. For example, if the model wrongly understands the context by assuming a “chicken” as a “roasted chicken” (see 1st sample), it becomes impossible to satisfy the prompt “a chicken tasting the sauce,” regardless of the strength of the motion model. This insight indicates a critical gap: Current T2V models may have **over-entangled** the two distinct tasks, static scene construction and temporal synthesis, yet are not structurally equipped to handle the first reliably.

To delve into and understand this gap, we explore a diagnostic study by comparing Text-to-Video (T2V), Image-to-Video without text prompts (I2V), and Image-to-Video with text prompts (I2V+text) models in Table 1, revealing two observations. T2V models frequently produce distributionally shifted frames yet still achieve FVD scores comparable to I2V models, indicating that **their motion modeling remains reasonably natural even when scene fidelity is relatively poor**. I2V models exhibit the complementary behavior, strong FID from accurate initial scenes and weaker temporal coherence, while I2V+text balances both aspects. This contrast suggests a **structural mismatch in current T2V models**: scene grounding and temporal synthesis benefit from distinct inductive biases, yet existing architectures attempt to learn both simultaneously within a single model.

These observations motivate us to revisit T2V. *Rather than formulating it as a single task, we factorize it into two fundamentally factorized sub-problems: specifying the initial scene and generating its temporal evolution.* A natural way to operationalize this separation is through a visual anchor defining the intended starting state of the video. However, such an anchor cannot be generated by simply running a Text-to-Image (T2I) model on the original video prompt, which often contains multi-stage actions or temporal transformations. Obtaining an appropriate anchor requires first clarifying the prompt’s intended initial condition.

Based on this insight, we propose Factorized Video Generation (FVG), a pipeline that explicitly decomposes T2V generation into specialized stages designed to address each subproblem independently: **(1) Reasoning:** A Large Language Model (LLM) rewrites the video prompt into an explicit description of the initial scene, removing temporal transitions and eliminating logical ambiguities. **(2) Composition:** A T2I model uses this refined prompt to synthesize a high-quality, semantically grounded anchor frame. **(3) Temporal synthesis:** A video diffusion model condi-

Table 1. Diagnostic study in understanding the over-entangled gap. FID/FVD of WAN 2.2 (5B) with 5k samples on two video generation datasets. We compare T2V, I2V, and I2V+text generations. I2V+text consistently achieves the best FID/FVD.

Metric	VidGen [45]			OpenVid-1M [30]		
	T2V	I2V	I2V+Text	T2V	I2V	I2V+Text
FID	14.10	10.12	5.25	17.28	8.56	3.33
FVD	178.76	142.12	34.78	28.99	124.58	27.08

tions on both the anchor and the original prompt, focusing exclusively on generating coherent temporal dynamics. The contributions of this work are as follows:

- Through qualitative and quantitative evaluation, we show that scene composition is one of the primary failure modes in existing T2V systems.
- We introduce FVG, a simple and modular factorization of T2V generation into reasoning, composition, and animation, enabling improved scene grounding and temporal coherence.
- We demonstrate that this decomposed approach sets a new state-of-the-art on the CompBench benchmark [35] and significantly improves all tested models on VBench2 [51].
- We show that visual anchoring enables significant reductions in sampling steps without degrading output quality, providing a practical path toward more efficient video generation.

We also release our models, code, benchmark prompts and image anchors generations to support reproducibility and facilitate further research.

2. Related Work

Image Generative Models. With systematic scaling of architectures and datasets, state-of-the-art image generation models [7, 9, 20, 32, 34, 43, 46], exemplified by the 20B-parameter Qwen-Image [46], achieve photorealistic synthesis with fine-grained controllability that flexibly adapts to user specifications. These models exhibit robust text-image alignment, semantic coherence, and comprehensive multi-modal editing capabilities [4, 13] in an efficient manner.

Video Generative Models. In parallel, video models [3, 5, 11, 21, 26, 49] have also made great progress in generating temporally coherent short contents, which can also be extended to minute-length long videos [10, 19, 28, 38, 44, 50]. However, compared with the image counterpart, introducing the extra temporal dimension presents fundamental challenges: Video data has *exponentially higher dimensionality* thus requires substantially richer text-video pairs, also leading to computational restrictions on model capacity. For example, current video models, such as Wan [42] (14B), remain significantly smaller than image counterparts like

Qwen-Image [46] (20B), limiting the semantic understanding. Consequently, existing models exhibit suboptimal text-following capabilities [14, 25], often resulting in missing concepts, temporal inconsistencies, and reduced prompt adherence compared to the image-generation counterparts.

Spatial-Temporal Factorization. To address the complexity in video-centric learning, factorization [40] has become a fundamental architectural strategy [2, 22, 27, 29], which decouples spatial and temporal components to enable efficient video representation. Some works [5, 6] extend this paradigm via hierarchical factorization across multiple scales. Due to the reduced model scale, these factorized approaches compromise spatial-temporal coupling, leading to suboptimal results when data is scaled [29]. *Differently, we propose a new perspective by lifting the architecture factorization to a higher task-oriented level*, thereby preserving model capacity while achieving superior text-following capabilities in video generation.

3. Preliminaries

Flow Matching for Denoising. Recent video diffusion models are grounded in the flow-matching formulation [17, 23, 24], which views denoising as learning a continuous-time flow field that maps a simple prior distribution, typically Gaussian, to the target data distribution. Given video latents $\mathbf{z}_0 \sim \mathcal{N}(0, \mathbf{I})$ and data samples $\mathbf{z}_1 \sim p_{\text{data}}(\mathbf{z})$, the model learns a vector field $\mathbf{v}_\psi(\mathbf{z}_\tau, \tau)$ that transports intermediate states $\mathbf{z}_\tau = \tau\mathbf{z}_1 + (1 - \tau)\mathbf{z}_0$ along time $\tau \in [0, 1]$:

$$\mathcal{L}(\psi) = \mathbb{E}_{\tau, \mathbf{z}_0, \mathbf{z}_1} \|\mathbf{v}_\psi(\mathbf{z}_\tau, \tau) - (\mathbf{z}_1 - \mathbf{z}_0)\|_2^2. \quad (1)$$

In practice, this formulation generalizes the discrete-step denoising process of diffusion models, where the continuous flow is approximated by T discrete denoising steps. A higher number of steps yields finer approximations of the flow trajectory but at a higher computational cost. Our study later explores how visual grounding improves robustness even when T is significantly reduced.

Conditioning Mechanisms. Conditioning guides the generation toward desired semantics or structure. Text prompts are typically encoded into embeddings h_y via a transformer encoder (e.g., T5 [33]) and injected into the model through cross-attention:

$$\mathbf{h}' = \text{Attention}(\mathbf{Q} = \phi(\mathbf{z}_t), \mathbf{K} = h_y, \mathbf{V} = h_y), \quad (2)$$

where $\phi(\mathbf{z}_t)$ denotes the query features from the current latent. For image conditioning, a reference frame \mathbf{x}_0 or its encoded features $h_{\mathbf{x}_0}$ are concatenated with the video latent representation, either channel-wise or in the temporal dimension:

$$\mathbf{z}'_t = [\mathbf{z}_t; h_{\mathbf{x}_0}], \quad (3)$$

allowing the model to anchor spatial structure before learning temporal evolution. This combination—text via cross-attention and image via concatenation is referred to as image-to-video (I2V) diffusion with text conditioning, enabling the model to generate semantics and scene layout jointly. However, such joint conditioning typically requires extensive retraining and substantial computational resources to align multimodal representations effectively.

4. Methods

The goal of this work is to investigate how grounding text-to-video (T2V) diffusion models with at least one visual anchor affects their performance on complex compositional tasks. By introducing a visual anchor, we aim to decouple video generation into two subtasks, scene context construction and temporal motion modeling, and evaluate whether this separation improves the model’s understanding of scenes, objects, and their interactions. Our focus extends beyond visual quality to assess reasoning-oriented capabilities of video diffusion models. To this end, we compare standard T2V models with their text–image–to–video (I2V+text) counterparts across benchmarks designed to evaluate compositional video generation. Furthermore, to enable a fair comparison within the same architecture, we propose dedicated finetuning and inference pipelines that integrate a visual anchor into a pure T2V model. The following section details these pipelines which are summarized in Sec. 2.

4.1. Anchor-Grounding Finetuning

A core capability required by the FVG pipeline is the ability to inject a visual anchor into a pretrained T2V diffusion model. We enable this through anchor-grounding finetuning, which teaches the model to treat the provided image as the initial frame of the generated video.

4.1.1. Latent Injection for Anchor Grounding

To enforce strong grounding, we directly intervene in the diffusion process by injecting the clean latent of the anchor image into the model’s noisy latent sequence, inspired by diffusion-based inpainting methods [31]. Specifically, given a noisy video latent x_t containing T frames sampled at the same diffusion timestep t , we replace one frame with the clean latent of the anchor image (i.e., at timestep $t = 0$), forming a hybrid latent: $T - 1$ noisy frames at timestep t , 1 clean anchor frame at timestep 0.

This hybrid input is fundamentally out-of-distribution for a pretrained T2V model, which is trained exclusively on uniform-timestep sequences. Without any finetuning the method failed as the model failed to adapt to this hybrid input. However, we find that the model can reliably learn this behavior with lightweight LoRA finetuning, enabling it to interpret the $t = 0$ frame as a fixed visual constraint.

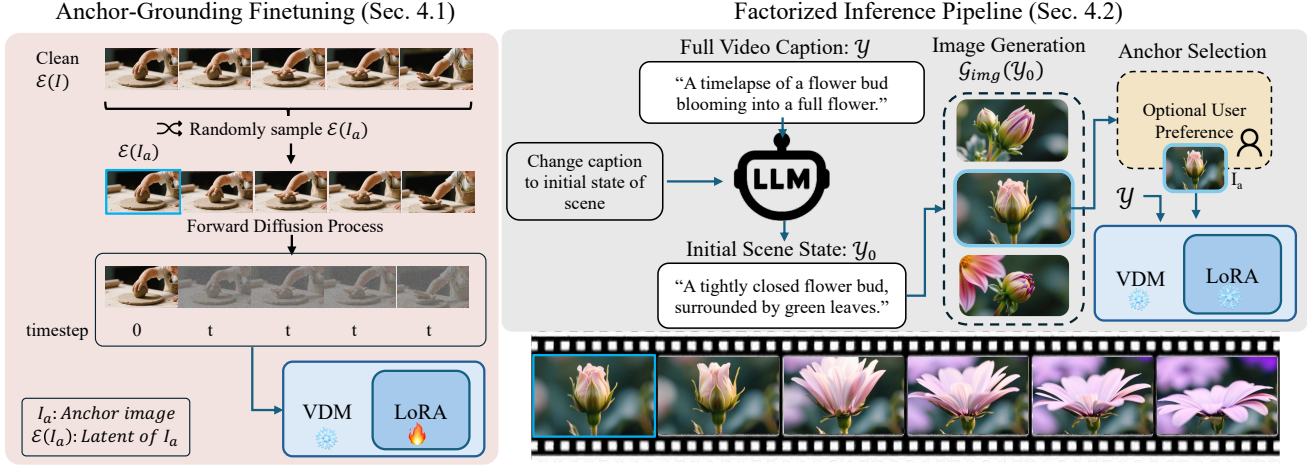


Figure 2. Overview of the finetuning and inference pipelines for our factorized video generation. Anchor-Grounding Finetuning: The Video Diffusion Model (VDM) is trained to follow a visual anchor by injecting a clean image latent at a randomly chosen frame position and setting its diffusion timestep to $t = 0$. Lightweight LoRA finetuning trains the model to treat this clean frame as a fixed scene constraint that guides the rest of the video. Factorized Inference Pipeline: a LLM modifies the video prompt into a first-frame descriptive prompt to generate an anchor image. The anchor is then injected into the VDM with the timestep fixed set to 0.

Algorithm 1 Anchor-Grounding Finetuning

Require: Pretrained model ϵ_θ , Video z_0 , Text y

- 1: $k \sim \text{Uniform}(1, T)$ {Random anchor frame index}
- 2: $z_a \leftarrow z_0[k]$
- 3: $t \sim \text{Uniform}(0, 1)$
- 4: $\epsilon \sim N(0, I)$ {Sample noise}
- 5: Construct z_t and t_{vec}
- 6: **for** $j = 1$ to T **do**
- 7: **if** $j == k$ **then**
- 8: $z_t[j] \leftarrow z_a$ {Inject clean anchor}
- 9: $t_{vec}[j] \leftarrow 0$
- 10: **else**
- 11: $z_t[j] \leftarrow (1 - t) \times z_0[j] + t \times \epsilon[j]$
- 12: $t_{vec}[j] \leftarrow t$
- 13: **end if**
- 14: **end for**
- 15: $\text{loss} \leftarrow \|\epsilon - \epsilon_\theta(z_t, t_{vec}, y)\|_2^2$

4.1.2. Training Procedure

The training procedure for adapting a T2V model to an anchored model is detailed in Algorithm 1. The core idea is to create a hybrid input (z_t, t_{vec}) that pairs $T-1$ noisy frames at timestep t with one clean anchor frame at $t = 0$. The model ϵ_θ is then finetuned via LoRA to denoise this out-of-distribution input, learning to treat the $t = 0$ frame as a ground-truth anchor. The model itself is still conditioned only on the text prompt y .

4.2. Factorized Inference Pipeline

At inference time, we generate a visual anchor from the input text prompt before initiating the video generation process. Given a video text prompt y , we use a large language model (LLM) to generate a plausible detailed description of the scene's initial state y_0 , which emphasizes spatial layout, appearance, and object configuration. This reformulated prompt y_0 is then passed to a pretrained image generation model \mathcal{G}_{img} to synthesize the anchor image $I_a = \mathcal{G}_{img}(y_0)$.

Optionally, user control can be introduced at this stage to select the preferred visual style or appearance for the anchor. The selected generated image I_a is subsequently encoded into its latent representation $\mathcal{E}(I_a)$. Then, we apply this learned behavior to perform anchored generation. We set the anchor frame $k = 0$ (first frame) and provide the desired anchor latent $z_a = \mathcal{E}(I_a)$. Then during the denoising process, at each step t_i , we reconstruct a hybrid input for the model by replacing the first frame of the current latent z_{t_i} with the clean anchor z_a . We similarly construct a hybrid timestep vector t_{vec} where $t_{vec}[0] = 0$ and all other elements are set to t_i . The model then predicts the flow using this modified input.

Formally, at each sampling step t , the model updates the video latents according to:

$$z_{t_{i-1}} = z_{t_i} - \Delta t \mathbf{v}_\theta(z_t, t_{vec}, y), \quad (4)$$

where \mathbf{v}_θ denotes the learned velocity field of the video diffusion model. This ensures that the denoising trajectory evolves consistently from the anchored visual state.

This inference procedure enables anchor-grounded generation without requiring architectural changes or additional

conditioning modules, allowing the model to produce visually consistent and semantically aligned videos while preserving controllability over scene initialization.

4.3. Implementation Details

We finetune Wan2.2-14B [41], CogVideo1.5-5B, and Wan2.1-1B [41] using LoRA modules with a rank of 256, applied to all layers of the diffusion backbone. Finetuning is performed on 5000 randomly sampled videos from the UltraVideo [48] dataset for 6k steps with effective batch size of 16. Training requires around 48 GPU hours for Wan-1B and CogVideo-5B, and 96 GPU hours for Wan-14B. Wan 5B model natively supports both text-only and text-image conditioning; therefore, no finetuning is applied.

5. Experiments

In this section, we start by defining our experimental setup followed by an explanation of the experiments conducted.

5.1. Experimental Setup

To obtain image anchors, each caption is first refined using QWEN2.5-7B-INSTRUCT [36] to produce a detailed “first-image caption” describing the initial scene state. This refined description is then passed to QWENIMAGE [37] to synthesize a high-quality anchor image that serves as the first frame for the video diffusion model.

Evaluation Benchmarks. We evaluate our models on two text-to-video generation benchmarks. T2V-CompBench [35] measures compositional control over objects, attributes, and actions, assessing how well a model integrates multiple concepts within a coherent scene. VBench 2.0 [51] provides a holistic evaluation across 18 metrics, grouped into five high-level categories: creativity, commonsense reasoning, controllability, human fidelity, and physics. These categories collectively capture both semantic and physical consistency in video generation.

5.2. Performance on Complex Tasks

Results on T2V-CompBench: As shown in Tab. 2 across all models, adding an anchor image consistently improves compositional performances. All smaller Factorized models (CogVideo 5B, Wan 5B and Wan 1B) outperform the larger Wan 14B T2V model. **Our factorized Wan 5B also outperforms commercial PixVerse-V3 baseline which is the best reported model on the benchmark.** This demonstrates that visual grounding substantially enhances scene and action understanding even in smaller-capacity models. Within each model family, the factorized version outperforms the original model. Notably, our lightweight anchor-grounded LoRA on WAN 14B reaches performance comparable its pretrained I2V 14B variant (0.661 vs.

0.666), despite requiring no full retraining.

Results on VBench2.0: We summarize in Tab. 3 the results on VBench 2.0, reporting the five aggregated metrics. The complete set of 18 underlying metrics is provided in the Appendix. We report only the composition score instead of the original creativity metric (the latter averages composition and diversity) and study the diversity specifically in Sec. 5.4. Across all architectures, factorizing T2V consistently improves every VBench metric except human fidelity, which shows a small decline even when using prompt upsampling. Similar to the observations on T2V-CompBench, our factorized Wan 5B outperforms the larger Wan 14B model, demonstrating that visual grounding is sometimes more beneficial than scaling. While performance gains are consistent, improvements on VBench are generally smaller than on T2V-CompBench. This is expected since VBench applies a stricter evaluation protocol as most metrics are binary (0 or 1 per video) with no partial credit. Nonetheless, the trend confirms that visual anchoring systematically enhances compositional reasoning and controllability even under stricter assessment criteria.

Qualitative Results. Figure 5 shows representative examples comparing text-only generation with our factorized approach. Anchored videos consistently exhibit more accurate scene composition, stronger object–attribute binding, and clearer temporal progression.

5.3. Robustness to Reduced Sampling Steps

We assess robustness to reduced diffusion steps by decreasing sampling from 50 to 30 and 15 for Wan5B and calculate the results on T2V Compbench based on 5 different seeds. As shown in Fig. 9, the text-only model degrades sharply: -3.5% at 30 steps and -17% at 15 steps. The upsampled variant follows a similar trend but appears even more unstable (-10.2% and -22.0%), largely because it starts from a higher baseline at 50 steps. In contrast, the factorized model remains effectively unchanged, with only $+1.2\%$ and $+0.3\%$ variation. Although reducing diffusion from 50 to 15 steps would theoretically yield a $3.3\times$ speedup, the full end-to-end pipeline—including anchor-image generation remains $2.1\times$ faster in wall-clock time (1'39 vs. 3'30). Despite this substantial reduction in compute, the factorized model preserves the same accuracy, indicating that stronger conditioning not only improves quality but also stabilizes the diffusion trajectory, enabling far more efficient sampling.

5.4. Impact on Diversity

We evaluate generation diversity under several experimental settings, with results reported in Tab. 4. For each variation we generate 25 videos per prompt and calculate the diversity metric introduced by Vbench2.0.

Table 2. T2V CompBench results averaged across 5 runs for seven evaluation categories. Best scores within each model group are in **bold**. The Avg. column shows relative change vs. the group’s T2V baseline in parentheses. We include the best-performing model on the benchmark, the proprietary PixVerse-V3 for reference.

Model	Mode	Consistent Attribute	Dynamic Attribute	Spatial Relationship	Motion Binding	Action Binding	Object Interaction	Generative Numeracy	Avg.
SOTA (PixVerse-V3)	—	0.706	0.062	0.598	0.287	0.872	0.831	0.607	0.566
WAN 2.2 (5B) [41]	T2V	0.814	0.177	0.577	0.257	0.487	0.629	0.419	0.480
	T2V (upsampled)	0.866	0.137	0.606	0.245	0.509	0.690	0.523	0.511 (+6.46%)
	Factorized T2V (Ours)	0.943	0.393	0.710	0.282	0.831	0.873	0.740	0.682 (+41.98%)
WAN 2.2 (14B) [41]	T2V	0.844	0.127	0.639	0.299	0.624	0.765	0.553	0.550
	T2V (upsampled)	0.897	0.084	0.643	0.291	0.675	0.762	0.605	0.565 (+2.73%)
	Factorized I2V + Text	0.927	0.217	0.680	0.320	0.850	0.886	0.781	0.666 (+21.09%)
	Factorized T2V (Ours)	0.929	0.183	0.696	0.328	0.839	0.891	0.757	0.661 (+20.18%)
CogVideo 1.5 (5B) [12]	T2V	0.762	0.191	0.491	0.252	0.308	0.491	0.305	0.400
	T2V (upsampled)	0.794	0.144	0.526	0.240	0.414	0.573	0.338	0.433 (+8.25%)
	Factorized T2V (Ours)	0.916	0.316	0.645	0.255	0.770	0.838	0.550	0.613 (+53.25%)
WAN 2.1 (1B) [41]	T2V	0.793	0.150	0.541	0.232	0.461	0.648	0.383	0.458
	T2V (upsampled)	0.871	0.117	0.590	0.244	0.572	0.684	0.470	0.507 (+10.72%)
	Factorized T2V (Ours)	0.920	0.384	0.656	0.262	0.790	0.844	0.402	0.608 (+32.75%)

Table 3. VBench 2.0 results averaged over five random seeds. We report four main evaluation categories, each aggregating 17 underlying metrics (see Appendix for the full breakdown). For reference, we also include results from the best-performing model on the benchmark, the proprietary Veo 3.

Model	Mode	Composition	Commonsense	Controllability	Human Fidelity	Physics	Avg.
SOTA (Veo 3)	—	0.696	0.695	0.470	0.869	0.693	0.685
WAN 2.2 (5B) [41]	T2V	0.488	0.635	0.268	0.826	0.527	0.549
	T2V (upsampled)	0.543 (+11.3%)	0.594 (-6.5%)	0.386 (+43.7%)	0.806 (-2.5%)	0.647 (+22.6%)	0.595 (+8.4%)
	Factorized T2V (Ours)	0.654 (+34.0%)	0.647 (+1.8%)	0.446 (+66.3%)	0.780 (-5.6%)	0.638 (+21.0%)	0.633 (+15.3%)
WAN 2.2 (14B) [41]	T2V	0.538	0.631	0.361	0.824	0.513	0.573
	T2V (upsampled)	0.557 (+3.6%)	0.630 (-0.1%)	0.434 (+20.3%)	0.812 (-1.5%)	0.670 (+30.7%)	0.621 (+8.3%)
	Factorized T2V (Ours)	0.708 (+31.6%)	0.645 (+2.2%)	0.473 (+31.1%)	0.721 (-12.5%)	0.685 (+33.7%)	0.646 (+12.8%)
CogVideo 1.5 (5B) [12]	T2V	0.465	0.506	0.180	0.758	0.446	0.471
	T2V (upsampled)	0.479 (+2.8%)	0.579 (+14.3%)	0.198 (+10.2%)	0.793 (+4.5%)	0.531 (+18.9%)	0.516 (+9.4%)
	Factorized T2V (Ours)	0.649 (+39.4%)	0.636 (+25.6%)	0.304 (+69.3%)	0.652 (-14.0%)	0.562 (+25.8%)	0.561 (+19.0%)

The standard diversity evaluation involves fixing a text prompt and varying the random seed. For a standard T2V model, this generates multiple videos from the same text. However, in our factorized pipeline, a single seed change affects both the anchor image generation (T2I stage) and the subsequent video diffusion model. To disentangle these two sources of variance, we define two settings. First, we vary the seed for the entire factorized pipeline. This captures the total diversity (variation in both scene and motion). This is reported as “Seeds” in Tab. 4. Second, we generate a single anchor image, fix it, and then vary the seed only for the video diffusion model. This isolates motion-level diversity. This is reported as “Single Image”. We observe that the full FVG pipeline yields diversity scores comparable to the baseline T2V model. Conversely, and as expected, fixing the anchor image and varying only the video model seed causes the diversity score to drop significantly. These experiments suggest that generation diversity could be usefully

Table 4. Diversity evaluation when varying seeds and prompts.

Model Variable	T2V Seeds	T2V Prompt Rephrasing	Factorized T2V (Ours) Single Image	Factorized T2V (Ours) Seeds
WAN 5B	0.578	0.816	0.2404	0.539
WAN 14B	0.531	0.742	0.348	0.513

disentangled into scene-level diversity, which dominates the total variance, and motion-level diversity, which represents variations in animation for a static scene. Finally, we evaluate an additional diversity enhancement strategy by using an LLM to rephrase prompts. For each original prompt, we generate 25 semantic variations and provide them to the models. This “Prompt Rephrasing” method, as shown in Tab. 4, significantly boosts diversity scores across all tested models, confirming that semantic-level variation is a potent source of diverse outputs.

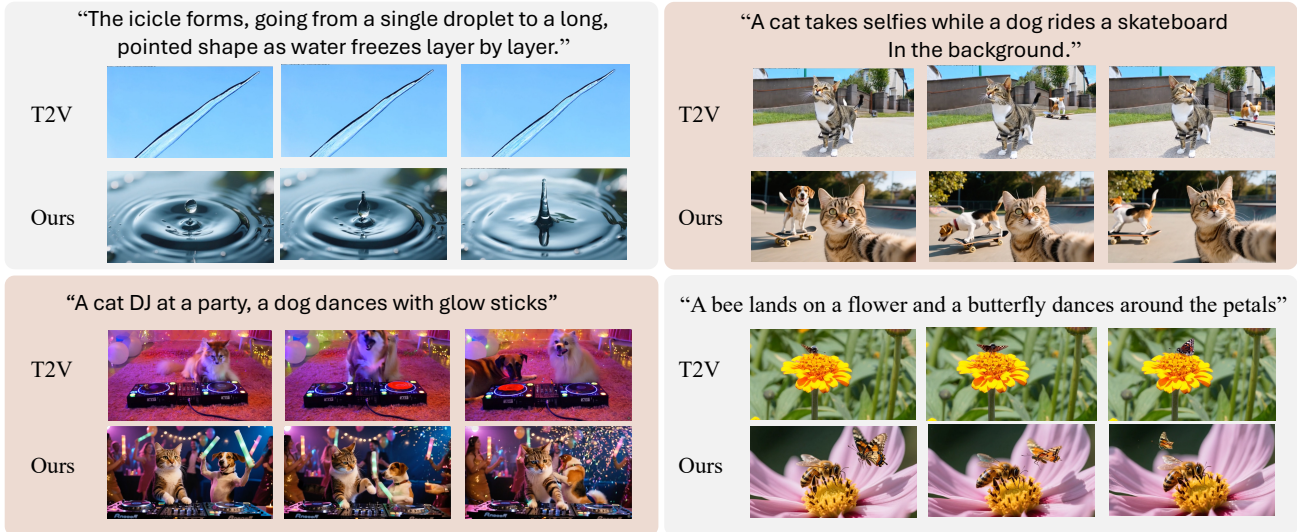


Figure 3. Qualitative results showing our factorized method leads to better performance. Additional results are provided in the appendix.

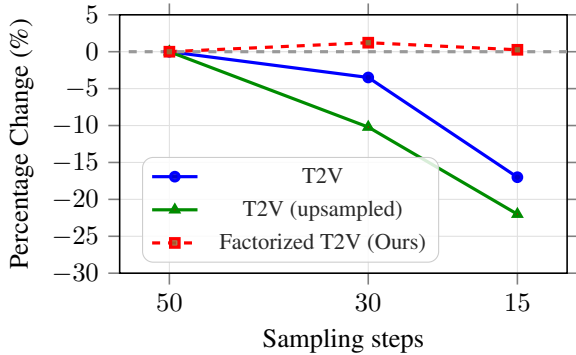


Figure 4. Percentage change in WAN 2.2 (5B) performance relative to the 50-step baseline. Both T2V variants degrade as steps decrease, while the factorized model remains stable even at 15 steps.

6. Ablation Studies

To better understand the components contributing to the effectiveness of factorized video generation, we conduct two ablations. First, we analyze the impact of the LLM-based prompt rewriting for anchor image generation. Second, we evaluate the model’s sensitivity to different anchor images.

6.1. Original Caption vs. LLM-based First-Frame Scene Description

We examine whether rewriting the video prompt using an LLM produces a more temporally appropriate anchor image—i.e., an image that correctly represents the scene as it should appear in the first frame. Specifically, we compare two settings on WAN 5B: (1) using the raw video caption directly as the image-generation prompt, and (2) us-

ing our LLM-refined first-frame description. On VBench 2.0, the direct-caption baseline achieves an average score of 55.8% which is to be compared to the T2V baseline of 54.9%. Our LLM-guided anchoring on the contrary reaches 63.3%, corresponding to a substantial relative improvement of 15.3%. These results highlight the importance of using an LLM to reason and generate a proper scene description. Providing a semantically accurate and temporally plausible starting scene is crucial. In contrast, using an unrefined caption often produces a mid-video moment, leading to weaker grounding and significantly lower overall performance (see qualitatives examples in Appendix).

6.2. Sensitivity to the Choice of Anchor Image

While our main experiments use a single preferred anchor image, mimicking a human-in-the-loop workflow, we also evaluate how sensitive the model is to the specific anchor provided. For Wan 5B, we generate five different anchor images per prompt using our LLM-refined first-frame description and assess the resulting videos across all VBench 2.0 categories. As shown in Tab. 5, the variation across different image anchors is extremely small: all categories have standard deviations below 0.02. This indicates that the slight variations resulting from the stochastic generation of anchor images affect mostly appearance and not the model’s compositional performance.

To contextualize this robustness, Tab. 5 compares the variability of our factorized model across anchors with the variability of the original T2V model across random seeds. On average, T2V is **9x more variable** with respect to seed than with respect to image anchors. This indicates the effectiveness of our factorized approach.

Table 5. Standard deviation across anchor images (Factorized Wan5B) vs. across seeds (Wan5B). Lower values indicate greater stability.

Category	Factorized Wan5B (Ours) (Std. Anchors)	Wan5B (Std. Seeds)
Consistent Attribute	0.0039	0.0117
Dynamic Attribute	0.0113	0.0203
Spatial Relationship	0.0092	0.1659
Motion Binding	0.0031	0.0053
Action Binding	0.0144	0.2180
Object Interaction	0.0128	0.2401
Generative Numeracy	0.0201	0.0171
Average	0.0107	0.0969

7. Discussion

Factorization vs. model scaling. Our results suggest that improved grounding, rather than increased capacity alone, may be equally important. Recent advances in T2V diffusion have relied heavily on increasing model size and training data, yet even large models often struggle to infer a coherent initial scene from text alone. This contrasts with image diffusion, where scaling is relatively straightforward; in video models, each architectural improvement must operate over an additional temporal dimension, making scaling substantially more resource intensive. Our findings indicate that improved grounding can complement scale by addressing a different bottleneck: establishing the correct scene before motion synthesis begins. By factorizing video generation into scene composition and temporal modeling, we mitigate several common failure modes without requiring substantially larger models. We view this as a complementary design principle that can guide future architectures toward more reliable and structured video synthesis.

Implications for T2V evaluation. The effectiveness of anchor-based generation also highlights a potential gap in current evaluation practices. Benchmarks such as VBBench2.0 and T2V-CompBench reward accurate scene composition and prompt adherence, yet we find that standard T2V models often underperform relative to a simple factorized baseline. This suggests that future evaluations may benefit from including anchor-conditioned baselines or I2V+text baselines to better disentangle scene construction from true temporal modeling. Ideally, to reflect improvements in motion understanding and generation of T2V models rather than their improvements in static composition, it would be valuable to evaluate their factorized version.

Performance on Human Fidelity. As shown in Tab. 3, both prompt upsampling and visual anchoring tend to reduce performance on the Human Fidelity category. This aggregate score combines three sub-metrics: human anatomy,

human clothes, and human identity. As detailed in the full results in Tab. 6 (Appendix), the decline is driven almost entirely by the human identity component, while the other two components remain stable. Through manual inspection, we observe that all model variants, regardless of anchoring, struggle to preserve identity especially across different actions. While our primary focus is improving compositional and reasoning capabilities, identity preservation is a distinct and challenging problem in its own. Addressing this limitation, potentially through explicit identity conditioning or persistent character representations, remains an important direction for future work.

On the diversity–correctness trade-off. Diversity is essential for applications such as synthetic data generation and counterfactuals, where one must produce multiple distinct videos without violating the intended scenario. Yet current diversity metrics rely on VGG feature differences, which primarily capture scene appearance. As shown in our performance ablation in Sec. 6.2, variability across seeds can meaningfully affect correctness, meaning that these metrics may interpret clear compositional failures or inconsistent layouts as “diversity”. Our factorized pipeline reduces prompt-adherence failures, as evidenced by its stronger benchmark scores, but while anchoring improves correctness, it does not guarantee diversity under current metrics. Conversely, standard T2V achieves higher numerical diversity but explores a broader but less controlled generative space, sometimes producing unfaithful or incorrect outcomes. We argue that the introduction of faithful diversity metric ensuring not only that the outputs vary but also that they respect certain constraints would be highly valuable. We also suggest that true video diversity should reflect two distinct diversity dimensions. First, the appearance diversity of the frames, which is captured with current metrics. Second, the motion diversity under given conditions. We argue that a possible principled way to evaluate motion diversity is to quantify the variability in a factorized model’s outputs when the first frame is kept constant, isolating motion from scene composition.

8. Conclusion

We proposed Factorized Video Generation, a simple pipeline that grounds the first frame before synthesizing motion, addressing a key failure mode of current T2V models. This factorization yields strong gains on compositional and reasoning benchmarks, with small models outperforming larger baselines and maintaining accuracy at one-third the sampling steps. While challenges such as identity preservation remain, our results show that explicitly separating scene construction from temporal modeling is a powerful and practical direction for future video generation research.

9. Acknowledgments

This work was supported as part of the Swiss AI Initiative by a grant from the Swiss National Supercomputing Centre (CSCS) under project ID a144. The research was supported by Innosuisse – the Swiss Innovation Agency (Ref. 127.265 IP-ICT).

References

- [1] Omer Bar-Tal, Hila Chefer, Omer Tov, Charles Hermann, Roni Paiss, Shiran Zada, Ariel Ephrat, Junhwa Hur, Guanghui Liu, Amit Raj, et al. Lumiere: A space-time diffusion model for video generation. In *SIGGRAPH Asia*, 2024. 1
- [2] Gedas Bertasius, Heng Wang, and Lorenzo Torresani. Is space-time attention all you need for video understanding? In *Icm*, page 4, 2021. 3
- [3] Andreas Blattmann, Tim Dockhorn, Sumith Kulal, Daniel Mendelevitch, Maciej Kilian, Dominik Lorenz, Yam Levi, Zion English, Vikram Voleti, Adam Letts, et al. Stable video diffusion: Scaling latent video diffusion models to large datasets. *arXiv preprint arXiv:2311.15127*, 2023. 1, 2
- [4] Tim Brooks, Aleksander Holynski, and Alexei A Efros. Instructpix2pix: Learning to follow image editing instructions. In *Proceedings of the IEEE/CVF conference on computer vision and pattern recognition*, pages 18392–18402, 2023. 2
- [5] Tim Brooks, Bill Peebles, Connor Holmes, Will DePue, Yufei Guo, Li Jing, David Schnurr, Joe Taylor, Troy Luhman, Eric Luhman, Clarence Ng, Ricky Wang, and Aditya Ramesh. Video generation models as world simulators, 2024. 1, 2, 3
- [6] Haoxin Chen, Menghan Xia, Yingqing He, Yong Zhang, Xiaodong Cun, Shaoshu Yang, Jinbo Xing, Yaofang Liu, Qifeng Chen, Xintao Wang, et al. Videocrafter1: Open diffusion models for high-quality video generation. *arXiv preprint arXiv:2310.19512*, 2023. 3
- [7] Junsong Chen, Jincheng Yu, Chongjian Ge, Lewei Yao, Enze Xie, Yue Wu, Zhongdao Wang, James Kwok, Ping Luo, Huchuan Lu, et al. Pixart-alpha: Fast training of diffusion transformer for photorealistic text-to-image synthesis. *arXiv preprint arXiv:2310.00426*, 2023. 2
- [8] Jiale Cheng, Ruiliang Lyu, Xiaotao Gu, Xiao Liu, Jiazheng Xu, Yida Lu, Jiayan Teng, Zhuoyi Yang, Yuxiao Dong, Jie Tang, et al. Vpo: Aligning text-to-video generation models with prompt optimization. *arXiv preprint arXiv:2503.20491*, 2025. 1
- [9] Patrick Esser, Sumith Kulal, Andreas Blattmann, Rahim Entezari, Jonas Müller, Harry Saini, Yam Levi, Dominik Lorenz, Axel Sauer, Frederic Boesel, et al. Scaling rectified flow transformers for high-resolution image synthesis. In *Forty-first international conference on machine learning*, 2024. 2
- [10] Songwei Ge, Thomas Hayes, Harry Yang, Xi Yin, Guan Pang, David Jacobs, Jia-Bin Huang, and Devi Parikh. Long video generation with time-agnostic vqgan and time-sensitive transformer. In *ECCV*, 2022. 2
- [11] Jonathan Ho, Tim Salimans, Alexey Gritsenko, William Chan, Mohammad Norouzi, and David J Fleet. Video diffusion models. In *NeurIPS*, 2022. 1, 2
- [12] Wenyi Hong, Ming Ding, Wendi Zheng, Xinghan Liu, and Jie Tang. Cogvideo: Large-scale pretraining for text-to-video generation via transformers. In *ICLR*, 2023. 6
- [13] Yi Huang, Jiancheng Huang, Yifan Liu, Mingfu Yan, Jiaxi Lv, Jianzhuang Liu, Wei Xiong, He Zhang, Liangliang Cao, and Shifeng Chen. Diffusion model-based image editing: A survey. *IEEE Transactions on Pattern Analysis and Machine Intelligence*, 2025. 2
- [14] Ziqi Huang, Yinan He, Jiashuo Yu, Fan Zhang, Chenyang Si, Yuming Jiang, Yuanhan Zhang, Tianxing Wu, Qingyang Jin, Nattapol Chanpaisit, Yaohui Wang, Xinyuan Chen, Limin Wang, Dahua Lin, Yu Qiao, and Ziwei Liu. Vbench: Comprehensive benchmark suite for video generative models. In *CVPR*, 2024. 3
- [15] Ziqi Huang, Yinan He, Jiashuo Yu, Fan Zhang, Chenyang Si, Yuming Jiang, Yuanhan Zhang, Tianxing Wu, Qingyang Jin, Nattapol Chanpaisit, et al. Vbench: Comprehensive benchmark suite for video generative models. In *CVPR*, pages 21807–21818, 2024. 1
- [16] Z. Huang et al. Storydiffusion: Consistent self-attention for long-range image and video generation. 2024. 1
- [17] Seungjun Kim, Minho Oh, Jihyong Park, Hyeonho Jeong, Jaehyeong Lee, Namil Kang, Youngjung Moon, and Sunghun Cho. Flowvid: Taming imperfect optical flow for consistent video diffusion. *arXiv preprint arXiv:2405.14867*, 2024. 3
- [18] Daeun Lee, Jaehong Yoon, Jaemin Cho, and Mohit Bansal. Videorepair: Improving text-to-video generation via misalignment evaluation and localized refinement. *arXiv preprint arXiv:2411.15115*, 2024. 1
- [19] Wuyang Li, Wentao Pan, Po-Chien Luan, Yang Gao, and Alexandre Alahi. Stable video infinity: Infinite-length video generation with error recycling. *arXiv preprint arXiv:2510.09212*, 2025. 2
- [20] Zhimin Li, Jianwei Zhang, Qin Lin, Jiangfeng Xiong, Yanxin Long, Xinch Deng, Yingfang Zhang, Xingchao Liu, Minbin Huang, Zedong Xiao, et al. Hunyuan-dit: A powerful multi-resolution diffusion transformer with fine-grained chinese understanding. *arXiv preprint arXiv:2405.08748*, 2024. 2
- [21] Bin Lin, Yunyang Ge, Xinhua Cheng, Zongjian Li, Bin Zhu, Shaodong Wang, Xianyi He, Yang Ye, Shenghai Yuan, Luhuan Chen, et al. Open-sora plan: Open-source large video generation model. *arXiv preprint arXiv:2412.00131*, 2024. 1, 2
- [22] Ji Lin, Chuang Gan, and Song Han. Tsm: Temporal shift module for efficient video understanding. In *Proceedings of the IEEE/CVF international conference on computer vision*, pages 7083–7093, 2019. 3
- [23] Yaron Lipman, Ricky T. Q. Chen, Haggai Ben-Hamu, Maximilian Nickel, and Matthew Le. Flow matching for generative modeling. In *Advances in Neural Information Processing Systems (NeurIPS)*, 2022. 3
- [24] Shitong Liu, Mingbo Gong, Xinyue Zhang, Bing Liu, Yang Song, Diederik P. Kingma, and Kihyuk Lee. Flow matching:

A unifying perspective of score-based diffusion and likelihood training. *arXiv preprint arXiv:2302.00482*, 2023. 3

[25] Yaofang Liu, Yumeng Ren, Xiaodong Cun, Aitor Artola, Yang Liu, Tieyong Zeng, Raymond H Chan, and Jean-michel Morel. Redefining temporal modeling in video diffusion: The vectorized timestep approach. *arXiv preprint arXiv:2410.03160*, 2024. 3

[26] Yixin Liu, Kai Zhang, Yuan Li, Zhiling Yan, Chujie Gao, Ruoxi Chen, Zhengqing Yuan, Yue Huang, Hanchi Sun, Jianfeng Gao, et al. Sora: A review on background, technology, limitations, and opportunities of large vision models. *arXiv preprint arXiv:2402.17177*, 2024. 1, 2

[27] Ze Liu, Jia Ning, Yue Cao, Yixuan Wei, Zheng Zhang, Stephen Lin, and Han Hu. Video swin transformer. In *Proceedings of the IEEE/CVF conference on computer vision and pattern recognition*, pages 3202–3211, 2022. 3

[28] Yu Lu, Yuanzhi Liang, Linchao Zhu, and Yi Yang. Freelong: Training-free long video generation with spectralblend temporal attention. *NeurIPS*, 37:131434–131455, 2024. 2

[29] Xin Ma, Yaohui Wang, Gengyun Jia, Xinyuan Chen, Zizheng Liu, Yuan-Fang Li, Cunjian Chen, and Yu Qiao. Latte: Latent diffusion transformer for video generation. *arXiv preprint arXiv:2401.03048*, 2024. 3

[30] Kepan Nan, Rui Xie, Penghao Zhou, Tiehan Fan, Zhenheng Yang, Zhijie Chen, Xiang Li, Jian Yang, and Ying Tai. Openvid-1m: A large-scale high-quality dataset for text-to-video generation. In *The Thirteenth International Conference on Learning Representations*. 2

[31] Haomiao Ni, Bernhard Egger, Suhas Lohit, Anoop Cherian, Ye Wang, Toshiaki Koike-Akino, Sharon X. Huang, and Tim K. Marks. Ti2v-zero: Zero-shot image conditioning for text-to-video diffusion models. In *2024 IEEE/CVF Conference on Computer Vision and Pattern Recognition (CVPR)*, pages 9015–9025, 2024. 3

[32] Dustin Podell, Zion English, Kyle Lacey, Andreas Blattmann, Tim Dockhorn, Jonas Müller, Joe Penna, and Robin Rombach. Sdxl: Improving latent diffusion models for high-resolution image synthesis. *arXiv preprint arXiv:2307.01952*, 2023. 2

[33] Colin Raffel, Noam Shazeer, Adam Roberts, Katherine Lee, Sharan Narang, Michael Matena, Yanqi Zhou, Wei Li, and Peter J. Liu. Exploring the limits of transfer learning with a unified text-to-text transformer. *Journal of Machine Learning Research*, 21(140):1–67, 2020. 3

[34] Robin Rombach, Andreas Blattmann, Dominik Lorenz, Patrick Esser, and Björn Ommer. High-resolution image synthesis with latent diffusion models. In *CVPR*, 2022. 2

[35] Kaiyue Sun, Kaiyi Huang, Xian Liu, Yue Wu, Zihan Xu, Zhenguo Li, and Xihui Liu. T2v-compbench: A comprehensive benchmark for compositional text-to-video generation. In *Proceedings of the Computer Vision and Pattern Recognition Conference*, pages 8406–8416, 2025. 1, 2, 5

[36] Alibaba Qwen Team. Qwen2.5-vl-32b-instruct: Smarter and lighter vision-language model, 2025. 5

[37] Alibaba Qwen Team. Qwenimage: Vision-language image generation utility, 2025. 5

[38] Meituan LongCat Team, Xunliang Cai, Qilong Huang, Zhuoliang Kang, Hongyu Li, Shijun Liang, Liya Ma, Siyu Ren, Xiaoming Wei, Rixu Xie, et al. Longcat-video technical report. *arXiv preprint arXiv:2510.22200*, 2025. 2

[39] Ye Tian, Ling Yang, Haotian Yang, Yuan Gao, Yufan Deng, Jingmin Chen, Xintao Wang, Zhaochen Yu, Xin Tao, Pengfei Wan, Di Zhang, and Bin Cui. Videotetris: Towards compositional text-to-video generation. *arXiv preprint arXiv:2406.04277*, 2024. 1

[40] Du Tran, Heng Wang, Lorenzo Torresani, Jamie Ray, Yann LeCun, and Manohar Paluri. A closer look at spatiotemporal convolutions for action recognition. In *Proceedings of the IEEE conference on Computer Vision and Pattern Recognition*, pages 6450–6459, 2018. 3

[41] T. Wan et al. Wan: Open and advanced large-scale video generative models. *arXiv preprint arXiv:2503.20314*, 2025. 1, 5, 6

[42] Ang Wang, Baole Ai, Bin Wen, Chaojie Mao, Chen-Wei Xie, Di Chen, Feiwei Yu, Haiming Zhao, Jianxiao Yang, Jianyuan Zeng, et al. Wan: Open and advanced large-scale video generative models. *arXiv preprint arXiv:2503.20314*, 2025. 2

[43] Xinlong Wang, Xiaosong Zhang, Zhengxiong Luo, Quan Sun, Yufeng Cui, Jinsheng Wang, Fan Zhang, Yueze Wang, Zhen Li, Qiyi Yu, et al. Emu3: Next-token prediction is all you need. *arXiv preprint arXiv:2409.18869*, 2024. 2

[44] Yuqing Wang, Tianwei Xiong, Daquan Zhou, Zhijie Lin, Yang Zhao, Bingyi Kang, Jiashi Feng, and Xihui Liu. Loong: Generating minute-level long videos with autoregressive language models. *arXiv preprint arXiv:2410.02757*, 2024. 2

[45] Yuxin Wang, Yifan Zhang, Rui Chen, Xiaolong Wang, and Dahua Lin. Vidgen: Benchmarking text-to-video generation with comprehensive evaluation metrics. In *Proceedings of the IEEE/CVF Conference on Computer Vision and Pattern Recognition (CVPR)*, 2024. 2

[46] Chenfei Wu, Jiahao Li, Jingren Zhou, Junyang Lin, Kaiyuan Gao, Kun Yan, Sheng-ming Yin, Shuai Bai, Xiao Xu, Yilei Chen, et al. Qwen-image technical report. *arXiv preprint arXiv:2508.02324*, 2025. 2, 3

[47] Youcan Xu, Zhen Wang, Jiaxin Shi, Kexin Li, Feifei Shao, Jun Xiao, Yi Yang, Jun Yu, and Long Chen. Como: Compositional motion customization for text-to-video generation, 2025. 1

[48] Zhucun Xue, Jiangning Zhang, Teng Hu, Haoyang He, Yinan Chen, Yuxuan Cai, Yabiao Wang, Chengjie Wang, Yong Liu, Xiangtai Li, et al. Ultravideo: High-quality uhd video dataset with comprehensive captions. *arXiv preprint arXiv:2506.13691*, 2025. 5

[49] Zhuoyi Yang, Jiayan Teng, Wendi Zheng, Ming Ding, Shiyu Huang, Jiazheng Xu, Yuanming Yang, Wenyi Hong, Xiaohan Zhang, Guanyu Feng, et al. Cogvideox: Text-to-video diffusion models with an expert transformer. In *ICLR*, 2025. 1, 2

[50] Lvmin Zhang and Maneesh Agrawala. Packing input frame context in next-frame prediction models for video generation. *arXiv preprint arXiv:2504.12626*, 2025. 2

[51] Dian Zheng et al. Vbench-2.0: Advancing video generation benchmark suite for intrinsic faithfulness, 2025. 1, 2, 5

Factorized Video Generation: Decoupling Scene Construction and Temporal Synthesis in Text-to-Video Diffusion Models

Supplementary Material

A. Flops Analysis

In this section, we give a more detailed study of the computation required by each model. The factorized version required a diffusion model for image generation and one for video generation. We report the Flops for a single call for each model. During sampling, the models are called multiple times for inference. As a video model, we report the Flops for Wan 2.2 with 5 billion parameters. For the image model, we report the Flops for Qwen-Image with 20 billion parameters. A single call of Wan 2.2 represents 117×10^3 GFLOPS. To generate a video, we use 50 inference steps and classifier-free guidance. As a result, the total cost of generating a video is 117×10^5 GFLOPS. A single call of Qwen-Image represents 10.7 GFLOPS. To generate an image, we use 50 inference steps and classifier-free guidance. As a result, generating an image costs about 10.7×10^2 GFLOPS. Finally, we use the factorized approach to reduce the number of inference steps from 50 to 15 for video generation. The total cost is 35.1×10^5 GFLOPS.

B. Detailed Experiments Results

B.1. VBench 2.0

Table 6 show the detailed metric results for VBench2.0 averaged across five seeds for Wan2.2 5B, Wan2.2 14B and CogVideo1.5 5B. Across the full set of 17 VBench2.0 metrics, we observe consistent trends that mirror the aggregated results in Tab. 3. First, factorized T2V improves nearly every metric relative to both T2V and upsampled T2V for all three model sizes (5B, 14B, and 5B CogVideoX). Improvements are especially significant in categories reflecting reasoning-driven scene understanding such as Composition, Instance Preservation, Motion Order Understanding, Dynamic Attribute and Dynamic Spatial Relationship further supporting our claim that anchoring mitigates the dominant failure mode of T2V: incorrect scene construction.

Second, we find that WAN 5B with anchoring often outperform WAN 14B T2V, despite having far fewer parameters. This confirms that scaling alone does not guarantee robust compositional reasoning, and that visual grounding provides a stronger foundation.

Third, consistent with our observations in Tab. 3, anchoring does not improve performance on Human Identity. The identity-related metric drops even when using upsampled prompts, indicating that this limitation stems from the underlying generative model.

Overall, the detailed metric breakdown reinforces that

anchoring strengthens video diffusion by correcting their weak scene construction and making use of their excellent temporal modeling which yields broad improvements in compositional correctness while remaining model and scale-agnostic.

B.2. Robustness to Reduced Sampling Steps

Table 7 and the full metric values reported in Table 8 show a clear difference in robustness of each model to a reduction in number of sampling steps. The text-only T2V model’s performance drops at 30 steps (-3.5% on average) and collapses at 15 steps (-17%), with large drop in categories such as Action Binding and Object Interaction. The upsampled T2V variant follows a similar pattern. Due to the fact that it begins with a higher 50-step baseline, its average performance decreases by -10.2% at 30 steps and -22.0% at 15 steps, with some metrics falling by over -35%. On the other hand, the factorized model remains remarkably stable. Even when the sampling steps are reduced to 30 or 15, its average score changes by only +1.22% and +0.26%, respectively. These results indicate that visual anchoring significantly improves robustness to aggressive step reduction. Thus, once the initial scene is grounded, generation relies far less on long denoising steps.

C. Qualitative Results

Anchored Scene Construction Across Multiple Video Models. Figure 5, Fig. 6, and Fig. 7 provides additional examples illustrating the visual differences between standard T2V generation and our factorized approach for Wan14B, Wan5B and CogVideo5B respectively across a wide variety of scenes. Across diverse prompts, the anchored model produces scenes with more accurate semantic alignment with the described situation. On the other hand, text-only T2V baselines often hallucinate or misinterpret spatial relations, or produce semantically incorrect first frames. These examples complement our quantitative results and highlight how grounding the visual anchor substantially improves scene construction.

Original Prompt vs. LLM-Refined First-Frame Prompt.

Figure 8 compares anchor images generated directly from the raw video prompt with those produced using the LLM-refined first-frame description. The refined prompts generate anchors that more accurately capture the intended initial configuration of objects, spatial layout, and contextual cues. Videos produced from these anchors exhibit stronger

Table 6. VBench 2.0 results averaged over five random seeds. We report raw per-metric scores, later aggregated into five categories.

Model	Mode	Camera Motion	Complex Landscape	Complex Plot	Composition	Dynamic Attribute	Dynamic Spatial Relationship	Human Anatomy	Human Clothes	Human Identity
SOTA (Veo3)	—	0.5494	0.2178	0.2187	0.6857	0.6374	0.4589	0.9026	0.9953	0.7084
WAN 5B	T2V	0.1630	0.1960	0.1156	0.4880	0.1319	0.3594	0.8811	0.9150	0.6826
	T2V (upsampled)	0.4963	0.2213	0.1279	0.5433	0.4066	0.3246	0.8763	0.9284	0.6133
	Factorized T2V	0.5685	0.2187	0.1677	0.6537	0.5670	0.4232	0.8904	0.8526	0.5967
WAN 14B	T2V	0.2148	0.1967	0.1443	0.5377	0.4872	0.4203	0.9266	0.8531	0.6919
	T2V (upsampled)	0.5407	0.1960	0.1592	0.5570	0.5659	0.3246	0.9294	0.9549	0.5509
	Factorized T2V	0.5741	0.2367	0.1796	0.7077	0.7473	0.3768	0.9310	0.8663	0.3653
CogVideoX 5B	T2V	0.2500	0.1880	0.0353	0.4655	0.1055	0.1507	0.5895	0.9050	0.7803
	T2V (upsampled)	0.2407	0.1693	0.0626	0.4786	0.1231	0.1797	0.7215	0.8371	0.8190
	Factorized T2V	0.2722	0.2227	0.1483	0.6490	0.2813	0.2754	0.7843	0.6306	0.5410

Model	Mode	Human Interaction	Instance Preservation	Material	Mechanics	Motion Order Understanding	Motion Rationality	Multi-View Consistency	Thermotics
SOTA (Veo3)	—	0.8067	0.9298	0.8411	0.8182	0.4040	0.4598	0.3595	0.7551
WAN 5B	T2V	0.6680	0.8807	0.4031	0.5848	0.2449	0.3897	0.5235	0.5976
	T2V (upsampled)	0.7880	0.7880	0.7348	0.6890	0.3354	0.4000	0.4751	0.6873
	Factorized T2V	0.7940	0.8316	0.7813	0.7768	0.3859	0.4621	0.3811	0.6125
WAN 14B	T2V	0.7675	0.8772	0.5916	0.5837	0.2929	0.3851	0.3025	0.5727
	T2V (upsampled)	0.8320	0.7851	0.8011	0.7464	0.4182	0.4759	0.4818	0.6513
	Factorized T2V	0.8100	0.8421	0.7436	0.8459	0.3838	0.4483	0.4354	0.7171
CogVideoX 5B	T2V	0.4600	0.7404	0.4271	0.6742	0.0670	0.2724	0.0969	0.5873
	T2V (upsampled)	0.5300	0.7439	0.6237	0.6438	0.0793	0.4138	0.2608	0.5946
	Factorized T2V	0.7420	0.8070	0.7587	0.7970	0.1859	0.4655	0.0150	0.6761

Table 7. Percentage change in WAN 5B performance when reducing sampling steps. The baseline results are at 50 sampling steps.

Model	Mode	Steps	Consistency	Dynamic	Spatial	Motion	Action	Interaction	Numeracy	Avg.
WAN 5B	T2V	15	-13.86	-14.62	-5.07	-6.93	-31.80	-20.34	-24.51	-17.00
	T2V	30	-2.44	-2.86	-0.13	1.10	-8.03	-3.54	-7.87	-3.49
	T2V (upsampled)	15	-19.00	10.72	-9.74	-2.36	-34.73	-27.38	-39.48	-22.01
	T2V (upsampled)	30	-8.71	12.48	-4.99	5.66	-14.01	-11.90	-26.16	-10.21
	Factorized T2V	15	0.26	-2.27	0.18	-1.66	0.03	2.96	-0.50	0.26
	Factorized T2V	30	0.02	0.68	0.16	-0.35	1.65	3.66	1.23	1.22

compositional fidelity and temporal coherence. This qualitative trend aligns with the quantitative improvements reported in Sec. 6.1.

Effect of Reduced Sampling Steps. Figure 9 illustrates how decreasing the number of diffusion steps affects visual quality. For text-only T2V models, fewer steps lead to degraded scene structure throughout the entire video. The factorized model preserves scene integrity even at 15 sampling steps. These results visually reinforce the stability trends observed quantitatively in Fig. 5, demonstrating that anchoring makes denoising far more robust to aggressive sampling reduction.

Comparison with Upsampled Text Figure 10 illustrates typical failure modes of prompt upsampling. Although upsampling produces more detailed text descriptions, it does not correct the underlying compositional weaknesses of T2V models as they seem to lead to similar problems in terms of semantic composition. Our factorized model resolves these cases by grounding generation in a concrete visual anchor. These examples highlight that text refinement alone cannot substitute for explicit scene grounding.

Table 8. Average WAN-5B results across five seeds for T2V, upsampled T2V, and our factorized T2V at different sampling steps. Our method remains stable even at 15 steps, whereas both T2V variants degrade sharply as steps decrease.

Model	Mode	Steps	Consistency	Dynamic	Spatial	Motion	Action	Interaction	Numeracy	Avg.
WAN 5B	T2V	15	0.7013	0.1515	0.5480	0.2391	0.3323	0.5008	0.3167	0.3985
	T2V	30	0.7943	0.1723	0.5765	0.2597	0.4481	0.6065	0.3865	0.4634
	T2V	50	0.8142	0.1774	0.5773	0.2569	0.4872	0.6287	0.4195	0.4802
	T2V (upsampled)	15	0.7013	0.1515	0.5468	0.2391	0.3323	0.5008	0.3167	0.3983
	T2V (upsampled)	30	0.7904	0.1539	0.5756	0.2587	0.4377	0.6075	0.3863	0.4586
	T2V (upsampled)	50	0.8658	0.1368	0.6059	0.2449	0.5090	0.6896	0.5232	0.5107
	Factorized T2V	15	0.9399	0.3836	0.6606	0.2799	0.8214	0.8953	0.7512	0.6760
	Factorized T2V	30	0.9377	0.3951	0.6604	0.2836	0.8347	0.9013	0.7642	0.6824
	Factorized T2V	50	0.9375	0.3925	0.6594	0.2846	0.8212	0.8695	0.7550	0.6742



Figure 5. Overall qualitative results comparing our factorized method against T2V methods. Visual examples from Wan14B showing that factorized T2V produces more coherent scene layouts and semantically aligned compositions than text-only T2V methods..

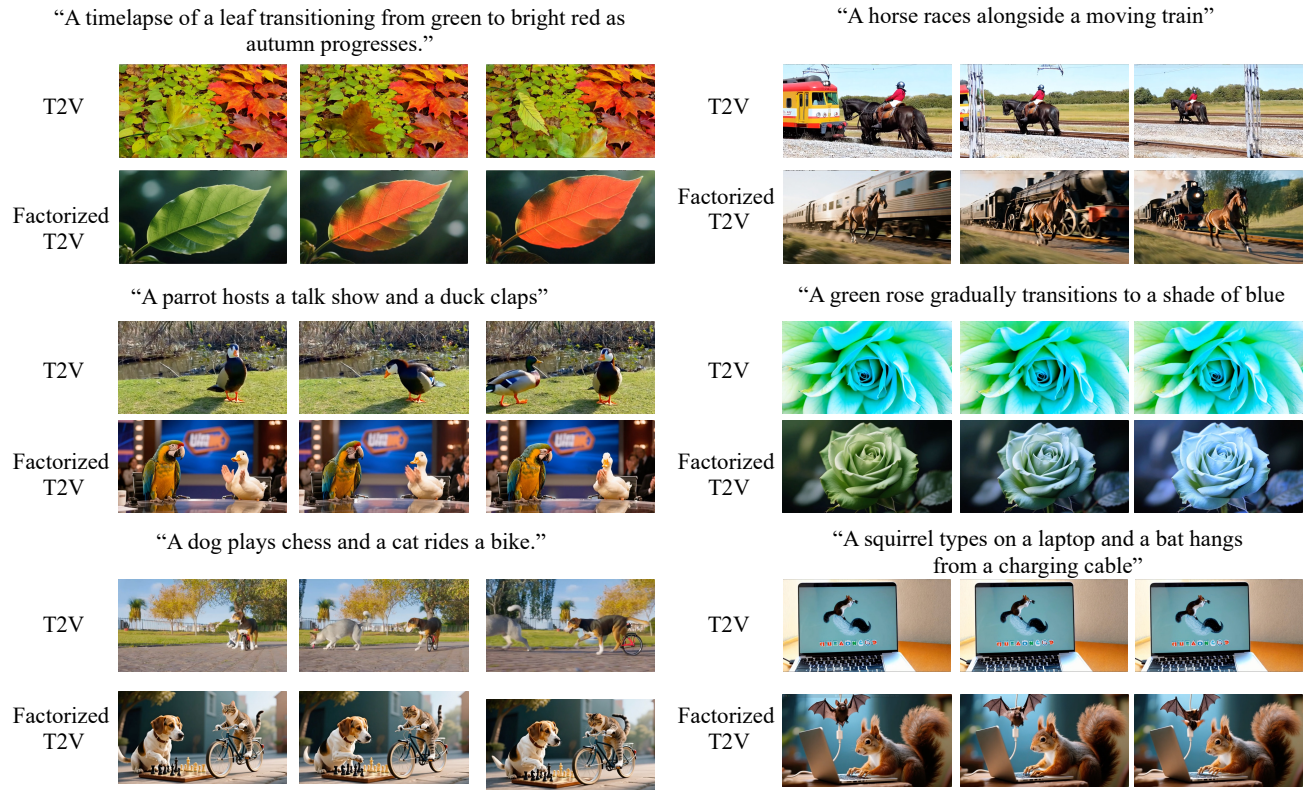


Figure 6. Overall qualitative results comparing our factorized method against T2V methods. Visual examples from Wan5B showing that factorized T2V produces more coherent scene layouts and semantically aligned compositions than text-only T2V methods..

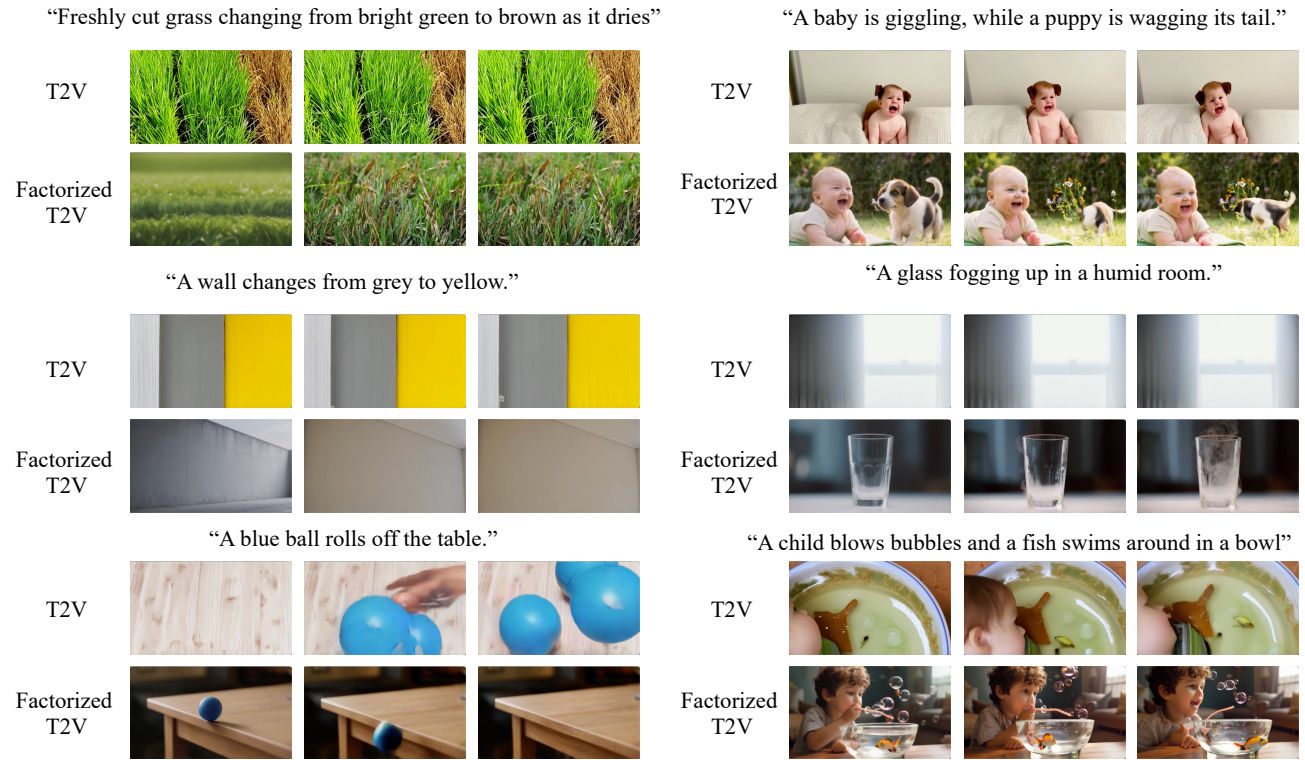


Figure 7. Overall qualitative results comparing our factorized method against T2V methods. Visual examples from CogVideo showing that factorized T2V produces more coherent scene layouts and semantically aligned compositions than text-only T2V methods.

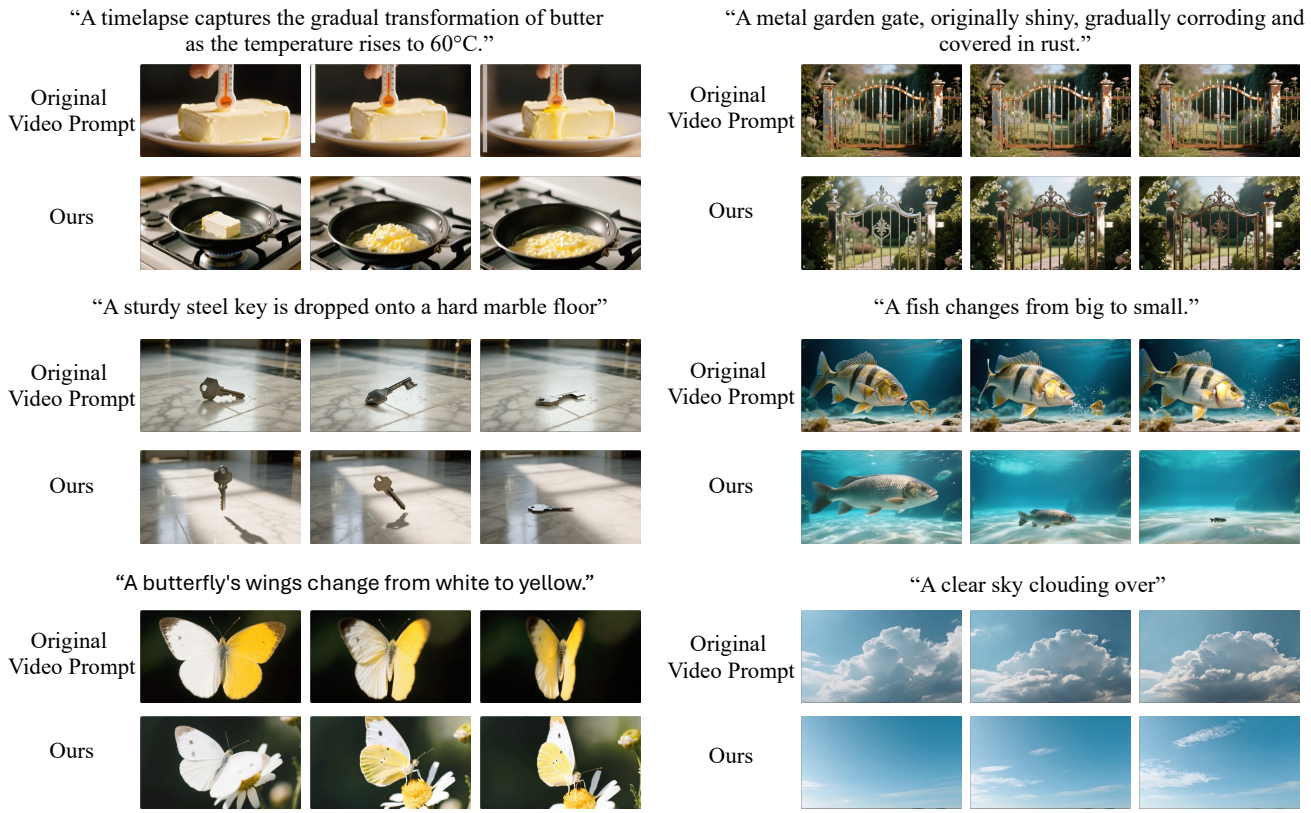


Figure 8. Effect of LLM prompt rewriting. Anchor images generated from LLM-refined first-frame descriptions more accurately reflect the intended initial scene than anchors produced from raw prompts.

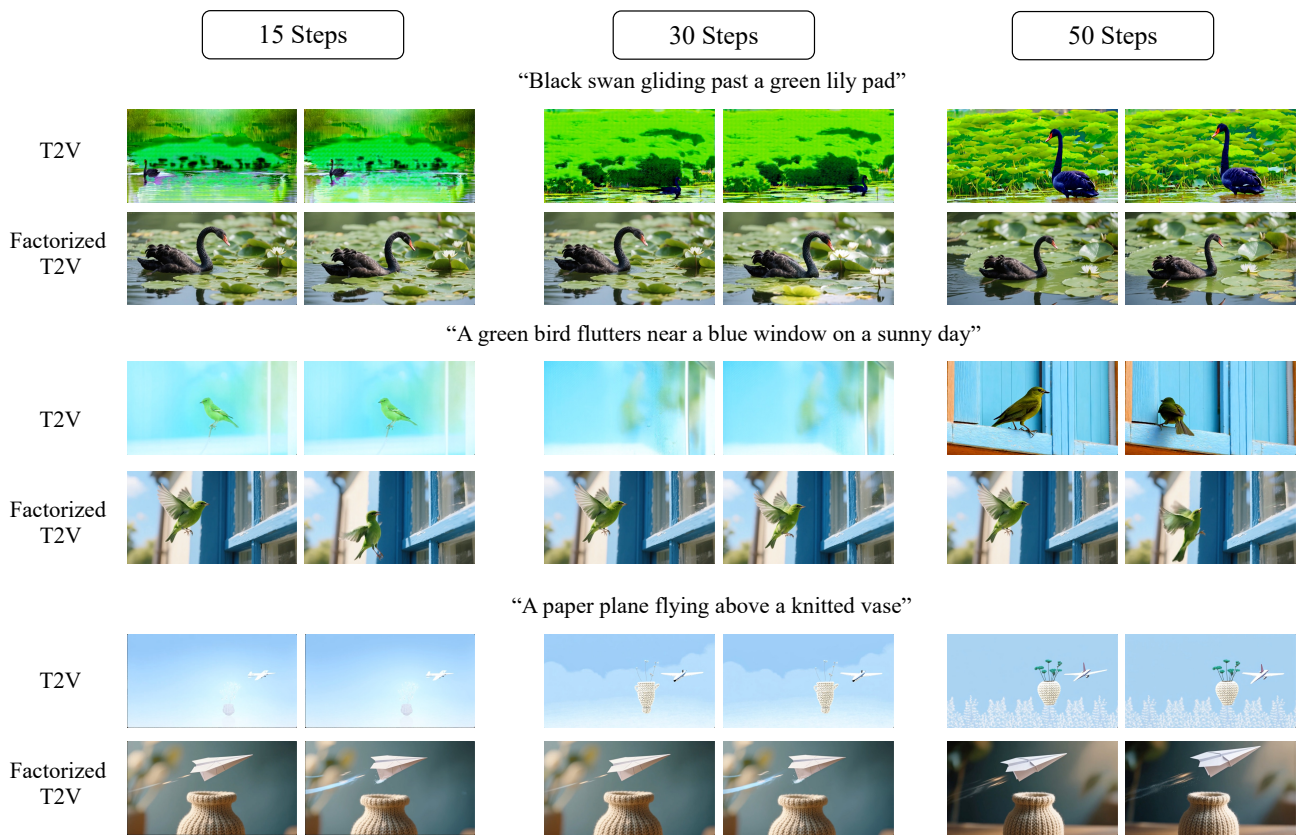


Figure 9. Qualitative sensitivity to sampling steps. Factorized T2V maintains coherent scene structure even at 15 steps, whereas text-only T2V collapses as sampling decreases.

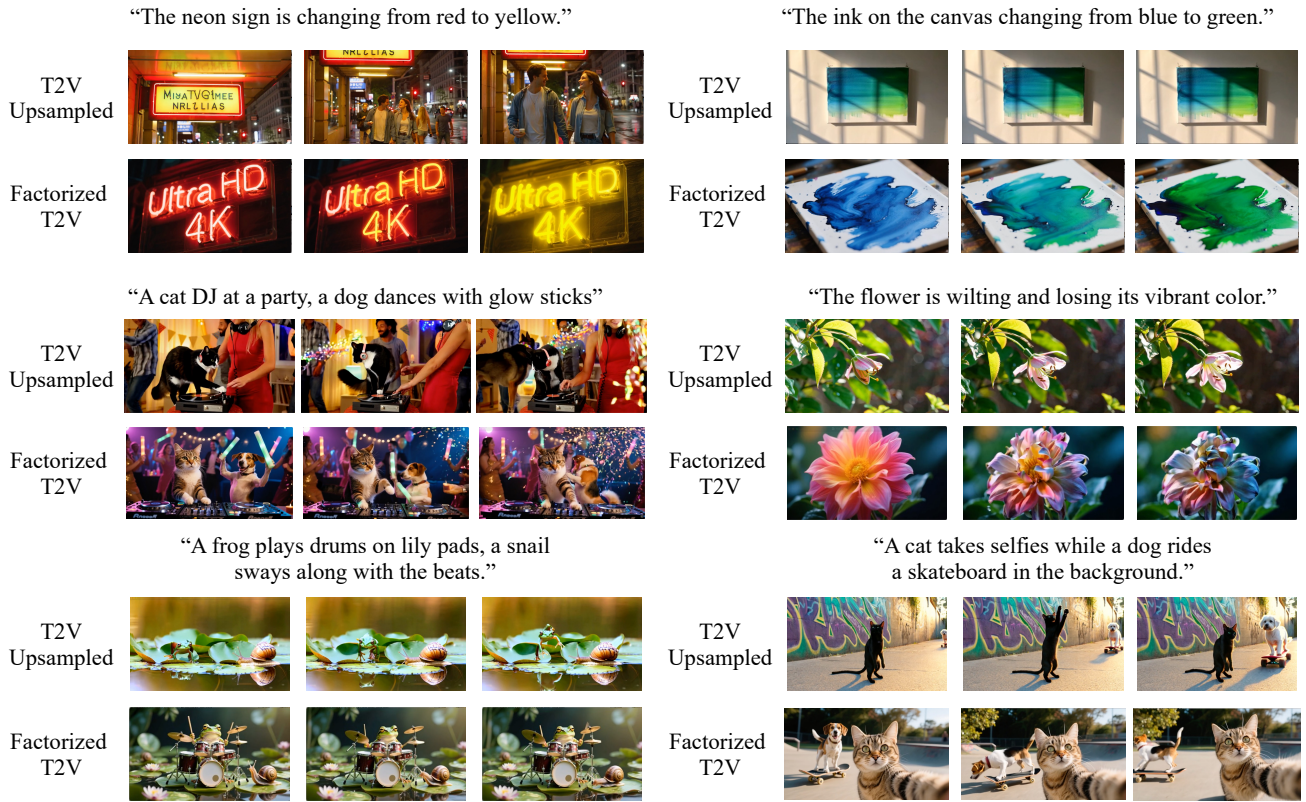


Figure 10. Prompt upsampling vs. factorized T2V. Upsampled T2V improves textual detail but does not fix core compositional failures. Our factorized model successfully reconstructs the correct scene structure across the same prompts.